Research Article SOHAG JOURNAL OF SCIENCES

https://doi.org/10.21608/sjsci.2024.295835.1208

The Effect of the Correction Term on the Equation of State of the Asymmetric Nuclear Matter(ANM) within the Bruckner-Hartree-Fock Approach

Alaa M. M. Ibrahim* and Khaled S. A. Hassaneen

Physics Department, Faculty of Science, Sohag University, Sohag 82524, Egypt
**Email: A.Ibrahim@science.sohag.edu.eg*

Received: 4th July 2024 **Revised:** 25th August 2024 **Accepted:** 28th August 2024
Published online: 9th September 2024

Abstract: The equation of state (EOS) of ANM by using the Bruckner-Hartree-Fock (BHF) approach enhanced by integrating a phenomenological 3-body force (3BF), contact term (CT) and Dirac corrections are investigated in this paper. In the present BHF calculations we used two types of realistic nucleon-nucleon (N-N) interactions. One is the charge-dependent Bonn potential (CD-Bonn) and the other is local soft core Argonne (V18). We can be used the EOS to obtain the bulk properties of nuclear matter such as the pressure, the incompressibility and the symmetry energy. The good agreement is observed when compared between the previous theoretical estimates and experimental data. After that we study the thermal properties of asymmetric nuclear matter such as the pressure at T= 0, 4, 8, 12, 16, 20, 24, 28 and 32 MeV. Also, a critical temperature T_c for asymmetric nuclear matter is found and there is no phase transition at high asymmetry parameter (α).
Keywords: Asymmetric Nuclear Matter, Equation of Sate, Thermal Properties, Critical temperature.

1. Introduction

The microscopic computations of asymmetric nuclear matter are significant in nuclear physics and astrophysics. The stellar structure equation (TOV equation) for a neutron star is fundamentally based on the properties of ANM, where it is determines the properties, such as the radius and the density profile of the neutron star and the maximum mass [1-3]. In addition to the general interest for the EOS of asymmetric nuclear matter in nuclear astrophysics, theoretical studies show that the properties (the binding energy, the radius and the thickness of neutron skins, the density distribution, and the deformation) of neutron-rich nuclei near the drop line depend sensitively on the isospin-dependent part of the equation of state for the nuclear matter [4-7]. Consequently, A microscopic theory of the structure of nuclei far from the valley of beta stability is being investigated through the study of asymmetric nuclear matter, which is the first step to this "hot" topic that is being produced by the rapid development of radioactive beam facilities.

This paper applies an approximation approach to ANM that is similar to the one that was developed [8]. Our work focuses on the effect of 3-body force on the bulk and single-particle properties in ANM using the BHF model. This advantage confirms that the thermodynamic consistency is satisfied in the BHF+3BF approach, e.g., the binding energy at saturation equals the chemical potential of the nucleons (Fermi energy) is usable.

2. The theoretical model

Z protons and N neutrons compose any ANM system, and they interact with one another via the strong nuclear interaction. The total density is given by $\rho=\rho_p+\rho_n$ and to the asymmetry parameter α= (N-Z)/A through the equations:

$$\chi_n = \frac{N}{A} = \frac{\rho_n}{\rho} = \frac{1+\alpha}{2}$$
$$\chi_p = \frac{z}{A} = \frac{\rho_p}{\rho} = \frac{1-\alpha}{2} \quad (1)$$

At first, we begin by building each of the G matrices of the BHF method of ANM, which describes the effective interaction between two nucleons when a medium is present [9-12]. They are gained by resolving the well-known Bethe-Goldstone equation.

$$\langle \vec{k}\,\vec{q}|G(\Omega)|\vec{k}\,\vec{q}\rangle_{\tau\tau'} = \langle \vec{k}\,\vec{q}|V|\vec{k}\,\vec{q}\rangle + \int d^3p_1\, d^3p_2 \langle \vec{k}\,\vec{q}|V|\vec{p_1}\,\vec{p_2}\rangle_{\tau\tau'} \times \frac{Q(p_1\tau,p_2\tau')}{\Omega-\left(e_{p_1,\tau}+e_{p_2,\tau'}\right)+i\eta}\langle \vec{p_1}\,\vec{p_2}|G(\Omega)|\vec{k}\,\vec{q}\rangle_{\tau\tau'} \quad (2)$$

The e_τ of a nucleon with momentum $\vec{k}$ is taken as

$$e_{k\tau} = \frac{k^2}{2m} + Re[\textstyle\sum_\tau^{BHF}(\vec{k},\omega = e_{k\tau})] \quad (3)$$

The "on-shell energy" G-matrix is used in the Bruckner-Hartree-Fock approach to calculate $U(\vec{k})$, which is produced by

$$U_\tau(\vec{k},\omega) = Re\textstyle\sum_\tau^{BHF}(\vec{k},\omega) = \sum_{\tau'}\int d^3q\langle \vec{k}\,\vec{q}|G(\Omega)|\vec{k}\,\vec{q}\rangle_{\tau\tau'} n_{\tau'}^0(\vec{q}) \quad (4)$$

This indicates that for ANM with a total density ρ and

asymmetry α.

$$\rho = \rho_p + \rho_n .$$

$$\alpha = \frac{\rho_n - \rho_p}{\rho} \quad (5)$$

this occupation probability is defined by

$$n_\tau^0(\vec{q}) = \begin{cases} 1 & for \ |\vec{q}| \le k_{F\tau} \\ 0 & for \ |\vec{q}| > k_{F\tau} \end{cases} \quad (6)$$

the total binding energy per nucleon can be expressed as

$$\frac{E}{A_{Total}} = \frac{E}{A_{BHF}} + \frac{E}{A_{3BF}} \quad (7)$$

where in BHF approach, the binding energy can be calculated as:

$$\frac{E}{A_{BHF}} = \sum \frac{3}{k_F^3} \int_0^{k_F} \frac{k^2}{2} \left[\frac{(k)^2}{2m} + e(k) \right] dk \quad (8)$$

In this work, the two-body force (2BF) of the realistic N-N interaction is used in the BHF calculation. It is completed by a 3BF of the Urbana type [13], which was reduced to a 2B density dependent force for use in BHF calculations by averaging over the third nucleon in the medium [14]. The two parameters (A and U) of the 3BF correction are determined by requiring that the BHF approach reproduces the energy and saturation density of SNM. The 3BF is expressed explicitly as the sum of two terms:

$$V_{ijk} = V_{ijk}^{2\pi} + V_{ijk}^{R} \quad (9)$$

The two - pion exchange contribution is a cyclic sum over the nucleon indices *i, j, k* of products of commutator [,] and anticommutator {,} terms

$$V_{ijk}^{2\pi} = A \sum_{cyc} (\{X_{ij}, X_{jk}\}\{\tau_i . \tau_j , \tau_j . \tau_k\} + \frac{1}{4} [X_{ij}, X_{jk}][\tau_i . \tau_j , \tau_j . \tau_k]) \quad (10)$$

Where

$$X_{ij} = Y(r_{ij})\sigma_i . \sigma_j + T(r_{ij}) S_{ij} \quad (11)$$

The repulsive part is defined by

$$V_{ijk}^{R} = U \sum_{cyc} T^2(r_{ij}) T^2(r_{jk}) \quad (12)$$

In the previous equations, the A and U parameters can be changed to reproduce the nuclear properties that are observed [15]. Two levels are involved when adding 3-body forces in BHF computations. The initial level, in a standard G-matrix calculation, the bare N-N interaction is enhanced with a density-dependent effective two-body interaction. Furthermore, the total energy must be modified to avoid match counting the 3BF contribution. [16, 17]. To do this, only at the lowest order can the Hartree-Fock (HF) contribution from 3BF be subtracted [18]:

$$\frac{E}{A_{3BF}} = \frac{E_{2BF}}{A} - \frac{1}{12} \frac{3}{k_F^3} \int_0^{k_F} k^2 dk \ \sum_{HF}^{3BF}(k) \quad (13)$$

Another correction, in nuclear matter in order to attain saturation properties, there is another method. BHF calculations must be supplemented by a simple contact interaction based on the Skyrme interaction at the mean field level for SNM [19].

$$\Delta H = \Delta H_0 + \Delta H_3 \quad (14)$$

where

$$\Delta H_0 = \frac{t_0}{8} [3 - \alpha^2] \rho \quad (15)$$

and

$$\Delta H_3 = \frac{t_3}{48} [3 - \alpha^2] \rho^{1+\gamma} \quad (16)$$

where t_0, t_3 and γ are free parameters and they represent the zero range and 3 -body strength, respectively. The parameter α is the asymmetry parameter (equal zero in SNM). We have fitted t_0 and t_3 by looking at certain properties or quantities and comparing their theoretical values with those known from experimental evidence.

The last correction**,** suggested corrections due to relativistic and other many-body effects [20]. The lowest order relativistic correction to the binding energy per nucleon in nuclear matter can be calculated by modifying the self-energy of the scalar meson. It can be approximated as

$$(\frac{E}{A})_{rel} \cong 2.4 \ (\frac{\rho}{\rho_0})^{8/3} \quad \text{MeV for ANM} \quad (17)$$

where ρ_0 is taken 0.17 fm^{-3}. We can obtain the Dirac–Brueckner by adding this correction to the nonrelativistic Brueckner G-matrix calculation.

By Stocker and Küpper et al. [21] Statistical mechanics of interacting Fermi systems techniques have been used to generalize the expressions for the thermal parameters of SNM to finite temperatures [22], at low temperatures. The entropy density for ANM can be expressed explicitly as

$$S = 2T \ \sum_i a_i \rho_i \quad (18)$$

Where,

$$a_i = \frac{\pi^2}{2} \frac{m_i^*}{k_{F_i}^2} = \frac{\pi^2}{2} \frac{m_i^*}{(3\pi^2 \rho_i)^{2/3}}] \quad (19)$$

the free energy per nucleon is find by:

$$F = \frac{E}{A_{T=0}} - a_i(\rho) T^2 = \frac{E}{A_{T=0}} - \frac{T^2 \pi^2}{2} \sum_i \left[\frac{m_i^*(\rho_i)}{((3\pi^2 \rho_i)^{2/3})} \right] \quad (20)$$

also, we can calculate the pressure per nucleon in ANM by:

$$P = \rho^2 (\frac{\partial F}{\partial \rho}) \quad (21)$$

3. Results and discussion

3.1. The EOS of ANM

The binding energy per particle (E/A) of ANM is plotted as a function of the density (ρ) at different values of asymmetry parameter α (0.2, 0.4, 0.6 and 0.8) using CD-Bonn potential within the six approaches BHF, BHF+3BF, BHF+CT$_{\gamma=0.33}$, BHF+CT$_{\gamma=0.5}$, BHF+CT$_{\gamma=0.66}$ and BHF+Dirac is shown in Fig. (1). We can see that, the BHF approach is more attractive than the other approaches and the BHF+Dirac approach is more

repulsion than the other approaches. The EOS becomes more repulsive when the asymmetry parameter (α) increases. Also, we can note that, the saturation densities of ANM depend on α and

At the asymmetry parameter α=0.8 the EOS becomes an incremental function with the density. It is also seen that, the 3BF has almost no effect on the EOS of ANM in the relatively low-density region. While at relatively high density, the 3BF provides a repulsive contribution to the EOS of ANM, and as increasing density, this repulsion from the 3BF becomes stronger and stronger.

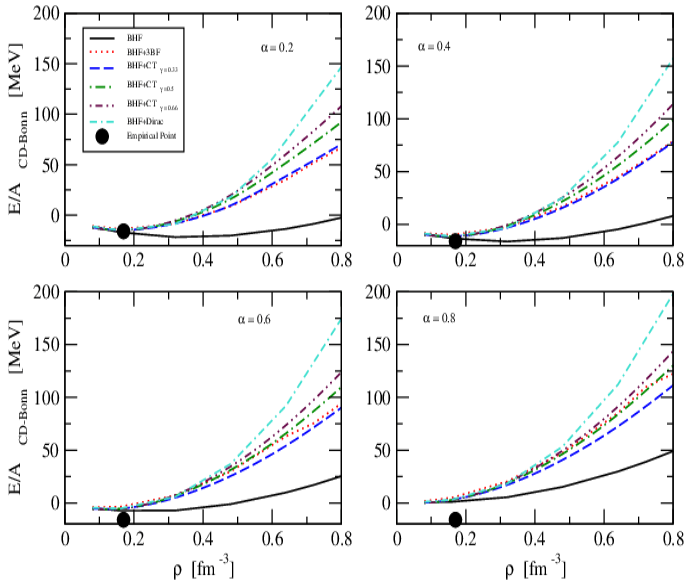

Figure 1: the E/A in MeV for ANM as a function of density ρ in fm^{-3} using CD-Bonn potential within BHF (solid line), BHF+3BF (dotted line), BHF+$CT_{\gamma=0.33}$ (short dashes), BHF+$CT_{\gamma=0.5}$ (dot-dashed line), BHF+$CT_{\gamma=0.66}$ (double dot-dashed line) and BHF+Dirac (double dashed-dot line) approaches.

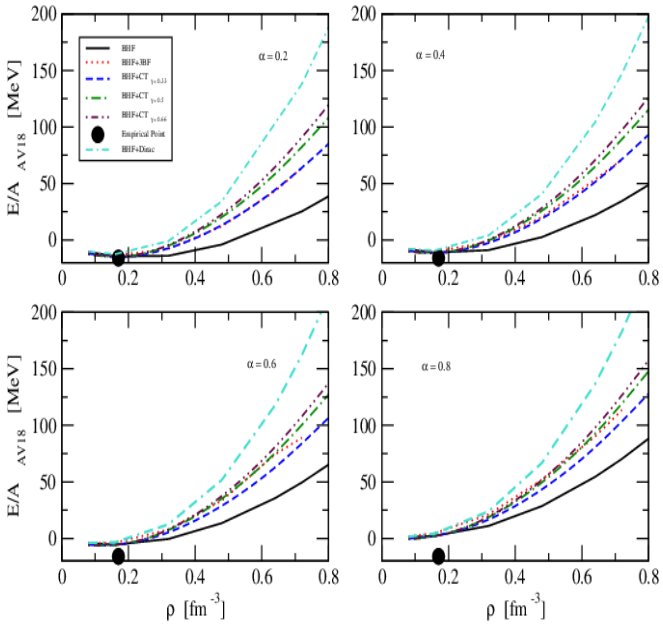

Figure 2: the E/A in MeV for ANM as a function of density ρ in fm-3 using AV18 potential within BHF (solid line), BHF+3BF (dotted line), BHF+CTγ=0.33 (short dashes), BHF+CTγ=0.5 (dot-dashed line), BHF+CTγ=0.66 (double dot-dashed line) and BHF+Dirac (double dashed-dot line) approaches.

Figure 2 is like to Figure 1 but using AV18 potential. One can see that, when α raises, the equation of state becomes more repulsive. Also, we can see that, the saturation densities of ANM change when the α changes and the saturation points shift to lower densities. Also, the inclusion of 3BF to BHF approach raises the repulsion of EOS. At the low densities, the difference between the six approaches is small but at the high densities this difference is increases with increasing the density.

In Tables 1 and 2 the equilibrium properties (i.e., calculated saturation properties) of ANM are summarized for the six approaches using CD-Bonn and AV18 potentials, respectively. One can see that, at the equilibrium density the compression modulus becomes smaller with the 3-body force despite its strong repulsive effect which enhances the curvature of the EOS. It goes back to the fact that it is also proportional to the square of the equilibrium density, which turns out to be very much reduced. Also, we can see that when the CT and Dirac corrections are added to the BHF calculations, the EOS becomes more repulsion than the other approaches.

Table 1: The saturation points as a function of density ρ are calculated using the CD-Bonn potential within BHF, BHF+3BF, BHF+$CT_{\gamma=0.33}$, BHF+$CT_{\gamma=0.5}$, BHF+$CT_{\gamma=0.66}$ and BHF+Dirac approaches at the different values of the asymmetry parameter α.

CD-Bonn

BHF			**BHF+3BF**	
α	**ρ_0 fm^{-3}**	**E/A_0 MeV**	**ρ fm^{-3}**	**E/A MeV**
0.2	0.36	-21.8	0.173	**-14.008**
0.4	0.305	-16.2	0.155	**-10.06**
0.6	0.248	-8.03	0.117	**-4.406**
BHF+$CT_{\gamma=0.3}$			**BHF+$CT_{\gamma=0.5}$**	
0.2	0.173	-14.6	0.155	**-14.756**
0.4	0.155	-11.2	0.155	**-11.37**
0.6	0.117	-5.80	0.117	**-6.054**
BHF+$CT_{\gamma=0.6}$			**BHF+Dirac**	
0.2	0.155	-14.8	0.192	**-15.21**
0.4	0.155	-11.4	0.173	**-11.47**
0.6	0.117	-6.09	0.136	**-5.602**

3.2. The thermal properties of ANM

We can see from Figs. 3 and 4 the relationship between the pressure as a function of the total density for various values of temperature (T= 0.0, 4.0, 8.0, 12.0, 16.0, 20.0, 24.0 and 28.0 MeV) at asymmetry parameter α = 0.2 within BHF, BHF+3BF, BHF+$CT_{\gamma=0.5}$ and BHF+Dirac approaches by using the CD-Bonn and AV18 potentials, respectively. we observed that, at low temperature, the pressure has a minimum. When T

increases, the minimum disappear, and the pressure increases with increasing the density ρ. At lower densities, we can see that the values of pressure are very sensitive to temperature and are independent of T at higher densities. The effect of the temperature decreases with increasing the asymmetry parameter. Also, when the asymmetry parameter increases, the repulsion of the pressure also increases. When 3BF added to the BHF calculations, the pressure becomes more repulsion than the pressure within BHF approach and the pressure by BHF+Dirac approach is more repulsion than the other approaches. Also, when we compare between two Figures, we can clearly see that the AV18 potential is more repulsion than the CD-Bonn potential.

From figures 3 and 4, we can see that the reasonable modify in the critical temperature T_c values which the critical temperature appears when the minimum of the curve will disappear. In this Table we can see the values of the critical temperature for all approaches. At the T_c, the pressure does not show any local minimum. This small change makes an important difference in the thermodynamical properties of nuclear matter. The values of the T_c follow by calculating the location of the minimum, searching for the condition that the minimum is zero, i.e. the critical temperature is calculated by [23],

$$T_c = \frac{5^{\frac{5}{6}}}{2^{\frac{13}{6}} 3^{\frac{1}{3}} b} \left(\frac{K_0}{m^*_0}\right)^{1/2} \rho_0^{\,-1/3} \quad (22)$$

where $b = \left(\frac{2^{\frac{5}{2}}\pi}{3\hbar^3}\right)^{1/3}$. In the previous formula, there is no explicit dependence on the saturation energy.

and

$$\left.\frac{\partial P}{\partial \rho}\right|_{T_c} = \left.\frac{\partial^2 P}{\partial^2 \rho}\right|_{T_c} = 0 \quad (23)$$

Table 2: The same as Table 1 but using the AV18 potential.

AV18

BHF			BHF+3BF	
α	ρ fm^{-3}	E/A MeV	ρ fm^{-3}	E/A MeV
0.2	0.23	-15.6	0.173	**-13.88**
0.4	0.211	-11.5	0.155	**-10.058**
0.6	0.155	-5.54	0.117	**-4.47**
	BHF+CT$_{\gamma=0.3}$			**BHF+CT$_{\gamma=0.5}$**
0.2	0.173	-14.7	0.155	**-14.87**
0.4	0.155	-11.3	0.155	**-11.52**
0.6	0.117	-5.99	0.117	**-6.35**
	BHF+CT$_{\gamma=0.6}$			**BHF+Dirac**
0.2	0.155	-14.8	0.155	**-12.56**
0.4	0.155	-11.5	0.136	**-9.31**
0.6	0.117	-6.30	0.117	**-4.33**

The value for the critical temperature depends strongly on the choice of the forces and approaches. The system only exists in the gas phase and the pressure becomes a monotonically increasing function of density, above the critical temperature. This behavior is observed in Figs. 3 and 4 for ANM by using the CD-Bonn and AV18 potentials. On the other hand, from these figures, we notice that the 3BF causes decrease of the T_c of ANM for the liquid-gas phase transition, after adding the 3BF the critical temperature is reduced to about 16.0 MeV. The values of the critical temperatures are listed in Table 3, and we can see from this table that when adding the contact term and Dirac corrections to the BHF calculations, the critical temperature doesn't affect. We can assume that this is because the contact term and Dirac corrections are not dependent on the effective mass.

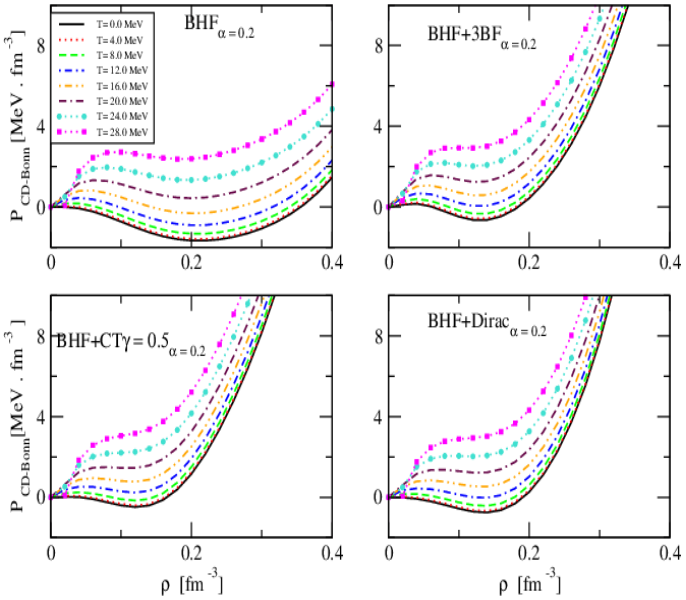

Figure 3: The pressure in MeV.fm^{-3} for ANM as a function of the density ρ in fm^{-3} using CD-Bonn potential within BHF, BHF+3BF, BHF+CT$_{\gamma=0.5}$ and BHF+Dirac approaches at asymmetry parameter α=0.2 and at temperatures T=0 (solid line), 4(dotted line), 8 (short dashes), 12(dot-dashed line), 16(double dot-dashed line), 20(double dashed-dot line), 24(circle-dot line) and 28MeV(square-dot line).

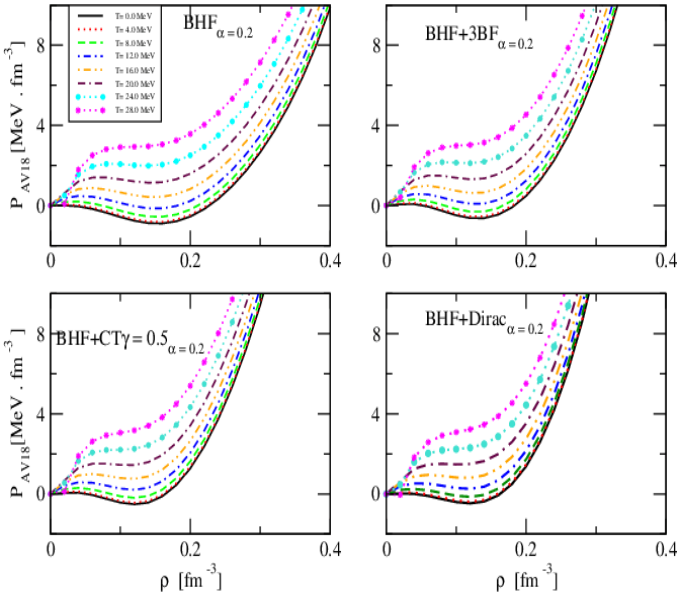

Figure 4: The same as Fig. 3 but using AV18 potential.

Table 3: the critical temperature values by using CD-Bonn and AV18 potentials within BHF, BHF+3BF, BHF+$CT_{\gamma=0.5}$ and BHF+Dirac approaches at asymmetry parameter α=0.2.

Model	A	T_c (MeV) CD-Bonn	T_c (MeV) AV18
BHF	0.2	24	20
BHF+3BF	0.2	16	16
BHF+$CT_{\gamma=0.5}$	0.2	20	20
BHF+Dirac	0.2	20	20

4. Conclusion

The bulk properties such as the EOS of ANM are studied in this paper at different values of the asymmetry parameter α= 0.2, 0.4, 0.6 and 0.8 using two N-N interaction within BHF, BHF + 3BF, BHF + $CT_{\gamma=0.33,\ 0.5\ \text{and}\ 0.66}$ and BHF+Dirac approaches. It is observed that the BHF approach is more attractive than the other approaches and the BHF+Dirac is more repulsion than the other approaches. Also, we can notice that the AV18 potential is more repulsive than the CD-Bonn potential. The saturation densities of ANM depend on the asymmetric parameter and at α=0.8 the EOS becomes an incremental function with density.

By using T^2-approximation, the predicted nuclear thermodynamics is entirely determined with no additional free parameters. The pressure is found to be strongly dependent on 3-body correlation and the liquid–gas coexistence region gets reduced in size when they are included. After calculated the EOS we used it to study the thermal properties of ANM at the different temperatures T= 4.0, 8.0, 12.0, 16.0, 20.0, 24.0 and 28.0 MeV within BHF, BHF + 3BF, BHF + $CT_{\gamma=0.33,\ 0.5\ \text{and}\ 0.66}$ and BHF+Dirac approaches at asymmetry parameter α=0.2. The pressure started decreasing with increasing the density and it becomes be zero at the saturation density and after the saturation density the pressure is increases with increasing the density. We can say that the effect of the contact term and Dirac corrections is less than the effect of the 3BF propagation on the critical properties of the liquid–gas phase transition

CRediT authorship contribution statement:

"Conceptualization, A.M.; software, A.M., K.S; formal analysis, A.M.; investigation, K.S.; data curation, K.S.; writing—original draft preparation, A.M.; writing—review and editing, A.M.; visualization, A.M.; supervision, K.S. All authors have read and agreed to the published version of the manuscript."

References

[1] I. Bombaci, Neutron Stars Structure and Nuclear Equation of State in Nuclear Methods and Nuclear Equation of State, 1st Ed. M. Boldo, World Scientific, Singapore, 1999.

[2] F. Weber and N. K. Glendenning, Rotating relativistic neutron stars, at the International Summer School on Nuclear Astrophysics, Tianjin, China, 1991.

[3] L. Engivik, M. Hjorth-Jensen, E. Osnes, G. Bao, E. Ostgaard, *Phys. Rev. Lett.*, 73 (1994) 2650.

[4] B. A. Li, C. M. Ko, and W. Bauer, *In. J. Mod. Phys. E*, 7 (1998) 147-229.

[5] I. Tanihata, *Nuclear Physics A*, 616 (1997) 56-68.

[6] H. Scheit, *et al.*, Phys. Rev. Lett., 77 (1996) 3967.

[7] M. Farine, T.Sami, B. Remaud and F. Sebille, Z.Phys. A 339 (1991) 363-366.

[8] K. S.A. Hassaneen, H.M. Abo-Elsebaa, E. A. Sultan, and H. M. M. Mansour, *Annals of Physics*, 326 (2011) 566-577.

[9] Hassaneen K.S.A. and Müther H., *Phys. Rev. C*, 70 (2004).

[10] K. Gad and K. S. A. Hassaneen, Nucl. Phys. A 793 (2007) 67.

[11] K. A. S. Hassaneen and K. j. Gad, Phys. Soc. Jpn., 77 (2008) 084201.

[12] P. Gögelein, E. N. E van Dalen, Kh. Gad, K. S. A. Hassaneen, and H. Müther, *Phys. Rev. C*, 79 (2009).

[13] J. Carlson, V. R. Pandharipande and R. B. Wiringa, *Nucl. Phys. A*, 401 (1983) 59-85.

[14].M. Baldo and L. S.Ferreira, Phys. Rev. C, 59 (1999) 682.

[15] M. Baldo, Nuclear Methods and the Nuclear Equation of State, International Review of Nuclear Physics World Scientific,Italy, 1999.

[16] K. Hebeler, A. Schwenk, *Phys. Rev. C*, 82 (2010) 014314.

[17] A. Carbone, Artur Polls and Arnau Rios, *Phys. Rev.C*, 98 (2018) 025804.

[18] F. Hugo Arellano, Felipe Isaule, and Arnau Rios, *Eur. Phys. J. A*, 52 (2016).

[19] P. Bonche, D. Vautherin, Nucl Phys. A, 372 (1981) 496.

[20] T. L. Ainsworth, E. Baron, G. E. Brown, J. Cooperstein, and M. Prakash, Nucl. Phys. A, 464 (1987) 740.

[21] W.Stocker, Phys. Lett. B 46 (1973) 59.

[22] A.A. Abrikosov, L. P. Gorkov, I. E. Dzialoshinski, and I. E. E. Dzialoshinskii, Methods of Quantum Field Theory in Statistical Physics,1st Ed, Prentice-Hall, Englewood Cliffs, new jersey,1963.

[23] A. Carbone, Artur Polls and Arnau Rios, *Phys. Rev.C*, 98 (2018) 025804.